Vacuum 175 (2020) 109251

Contents lists available at ScienceDirect

Vacuum

journal homepage: http://www.elsevier.com/locate/vacuum

Effect of silver ion implantation on surface physicochemical properties of composite materials based on polylactic acid and hydroxyapatite

O.A. Laput [a,*], D.A. Zuza [a,b], I.V. Vasenina [c], K.P. Savkin [b], I.A. Kurzina [a]

[a] National Research Tomsk State University, 36 Lenin Ave, Tomsk, 634050, Russia
[b] Institute of High Current Electronics, 2/3 Akademichesky Ave., Tomsk, 634055, Russia
[c] P.N. Lebedev Physical Institute, 53, Leninsky Prospect, Moscow, 119333, Russia

ARTICLE INFO

Keywords:
Polylactic acid
Hydroxyapatite
Composite materials
Ion implantation
Wettability
Degree of crystallinity
Cell viability
Biocompatibility

ABSTRACT

The investigation of surface physicochemical and biological properties of polylactic acid and hydroxyapatite and composite materials based on them modified by Ag 1×10^{15} ion/cm^2 and 1×10^{16} ion/cm^2 40 keV ion implantation is presented. X-ray analysis reveals that ion implantation of the above mentioned materials leads to crystallite size and degree of crystallinity increase. The intensity of -C = O line is found by IR-spectroscopy to be decreased that is associated with surface layer carbonization processes of PLA during ion implantation. Silver ion introducing is established to enhance hydrophobic properties of the materials; this process is accompanied by free surface energy decreasing. It is shown that cell viability of non-implanted PLA is comparable with a control sample and ion implantation negatively affects to cell viability. The investigated materials can be promising for biomedical application.

1. Introduction

Nowadays, ion-beam modification techniques become widely used since they include the complex of options: new material synthesis, surface composition modification, formation of predetermined pattern on surface, surface structure alteration, etc. Polymer and composite material investigation is related to a new and fast paced branch of modern science due to development of optimal materials for immune tolerant and biodegradable bone implants. Hence polymer and composite material of biomedical application are under close attention. Ion beam processing of various materials is one of the most important areas of modern industrial technologies due to a wide range of modes of treatment conditions [1,2]. The small depth of ion penetration contributes to the polymer surface functional property changes, while the bulk characteristics of the material are preserved.

Polymer materials have a low free surface energy while non-organic matrixes, in particularly, hydroxyapatite, in contrast are characterized by a high one, therefore, composite materials based on polymeric and inorganic components are increasingly used as materials for biomedical purposes. The average value of the free surface energy is necessary to preserve the vital activity of cells on the surface of the material that is embedded in the body. Biodegradable polymers based on lactic acid, used in medicine, have the hydrophobic surface, while a hydrophilic and at the same time well-developed surface is desirable for medical products for better adhesion of living cells. The main their disadvantages (poor adhesion characteristics, poor wettability) can be eliminated by implantation of ions of various types and energies in the subsurface layer [3]. Along with that, surface antibacterial effect can be obtained by silver ion implantation into the surface layer of the material, which also can increase the cell adhesion to the surface [4]. Investigation of the morphology and biocompatibility (in terms of antibacterial effect and cell proliferation) of polymer materials is an important step for clinical trials [5]. Composite materials based on polylactic acid (PLA) and hydroxyapatite (HA) may be promising materials for bone implantology. The structure and mechanical properties of composite biomaterials based on polylactic acid and hydroxyapatite (PLA/HA) are closest to the functional properties of natural bone tissue [6,7]. A continuous polymer matrix with finely distributed hydroxyapatite crystals is similar to the collagen component in bone tissue. The main idea of the polymer-non-organic composite material use is that polymer component of an implant reinforced with hydroxyapatite particles, which replaces a defected bone tissue, bioresorbs simultaneously with the process of forming a new bone tissue.

Complex physicochemical processes take place during the process of

* Corresponding author.
E-mail address: olesyalaput@gmail.com (O.A. Laput).

https://doi.org/10.1016/j.vacuum.2020.109251
Received 14 October 2019; Received in revised form 26 January 2020; Accepted 7 February 2020
Available online 11 February 2020

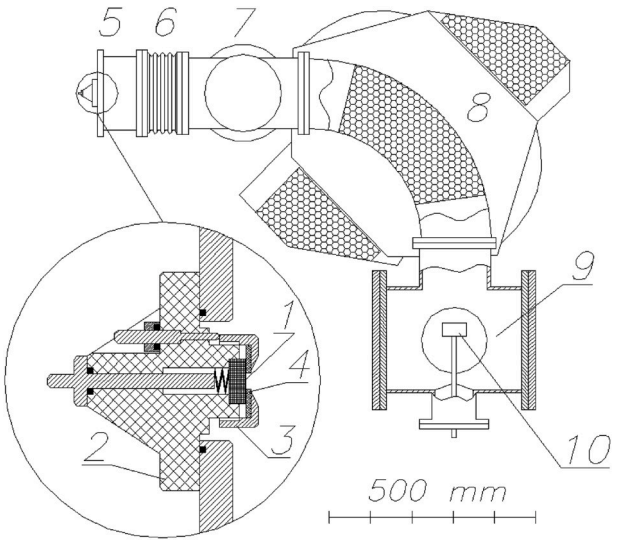

Fig. 1. Experimental setup: 1 – silver vacuum arc cathode; 2 – cathode holder; 3 – anode of trigger discharge; 4 – mica insulator; 5 – vacuum arc ion source; 6 – high voltage insulator; 7 – output chamber; 8 – bending magnet; 9 – input chamber; 10 – Faraday cup (Adopted from Ref. [20]).

ion-beam surface modification, which can significantly change the structure and properties of polymer surface, such as wettability, microhardness, conductivity, etc [8,9]. During ion implantation, the polymer bonds break, accompanied by the oxidation of the surface and the formation of new polar functional groups, which increase the hydrophilicity of the material. Surface treatment of polylactic acid films with cold plasma leads to an increase in roughness and wetting angle [10]. At the same time, an increase in roughness contributes to an improvement in the biocompatibility of polylactic acid [11]. In addition, it has been established [12,13] that when the surface of polylactic acid is irradiated with an electron beam, the length of the polymer chain changes, and the molecular weight and degree of crystallinity decrease in proportion to the increase in the radiation dose. In this paper, we investigate new composite materials with a unique surface treated on the basis of polylactic acid with hydroxyapatite. The effect of ion implantation on such materials has not previously been studied. Thus, this study is of an applied and fundamental interest related to practical application of surface-modified materials, as well as the physicochemical basis of the processes taking place in the surface layers of composite materials with polymeric and inorganic components. The purpose of this work is to study the effect of implantation of silver ions at the fluence of 1×10^{15} and 1×10^{16} ions/cm^2 on the physicochemical and biological properties of polymeric, ceramic, and composite materials based on polylactic acid and hydroxyapatite.

2. Materials and methods

2.1. Preparation of the experimental samples

Preparation techniques for PLA, HA and PLA/HA 80/20 composite material were described in detail elsewhere [14–16]. HA synthesis was carried out using the liquid-phase method with microwave radiation at pH ~11 according to the patented technology [17] by the equation:

$$10Ca(NO_3)_2 + 6(NH_4)_2HPO_4 + 8NH_3 \times H_2O \rightarrow Ca_{10}(PO_4)_6(OH)_2 + 20NH_4NO_3 + 6H_2O$$

Composite materials with dispersive hydroxyapatite were obtained by a mixture of PLA solution in chloroform (c = 0.1 g/ml) and HA powder at constant concentration; the mass proportion of components was 80/20. The choice of a composite with 80/20 ratio of PL/HA components follows from early studies, which found that this ratio displays optimal properties for this group of composites [18]. The suspension was treated with ultrasound with frequency 40 kHz for 20 min, and then precipitated in a fivefold excess of ethyl alcohol. The resulting fibers were dried in a drying oven at 40 °C until the solvent completely evaporated. The resulting composite material, as well as pure polylactic acid fibers, were subjected to mechanical grinding; then tablets with 10 mm diameter were formed with a PGR-10 hydraulic press at a pressure of 1×10^7 Pa.

2.2. Ion implantation

Ion implantation was done using a facility incorporating MEVVA II vacuum arc ion source [19] with a magnet separator [20] (Fig. 1). The beam was transported through the line of a bending magnet where its components with different mass-to-charge ratios were separated and focused. This implantation facility operates in a repetitively pulsed mode with repetition rate 1 Hz and pulse duration 300 μs. Charge state distributions of the ion beam were measured by a time-of-flight mass-to-charge spectrometer [21]. The separated beam of Ag^{2+} ions was used in the experiments. Since the ion source extraction voltage was 20 kV, the ion beam energy was 40 keV. Implantations were carried out to the fluence of 1×10^{15} and 1×10^{16} ions/cm^2. The implantation flux and average power density were adjusted by the ion beam current and pulse repetition rate, and were 5×10^{12} ions/(cm^2 × sec) and 1.5 mW/cm^2, respectively. The samples were mounted on a water-cooled target holder whose temperature did not exceed 20 °C. A working pressure of 1×10^{-6} Torr (1.3×10^{-4} Pa) was maintained by a pumping system based on two turbomolecular pumps.

2.3. Characterization techniques

The physicochemical properties of PLA, HA and PLA/HA 80/20 samples before and after Ag ion-beam treatment were studied including elemental and phase composition, morphology, wettability, and mechanical and functional properties. Chemical structure was investigated by infrared spectroscopy using a single attenuated total internal reflection (ATR-IR) attachment to a Nikolet 5700 IR-spectrometer. The elemental composition of the surface was studied by X-ray photoelectron spectroscopy (XPS) using a PHIX-tool automated XPS microprobe. Samples were mounted to the holder using conducting carbon or copper tape. For the XPS analysis, a monochromatic K_αAl X-ray source with an X-ray spot of 400 × 400 μm^2 was used. In the analysis, a standard charge compensation system with low electron and ion energy (≈0.1 eV) was used. Samples were cleaned by the Monatomic and Gas Cluster Ion Source (MAGCIS). X-ray photoelectron spectroscopy (XPS) is based on the photoelectric effect using monochromatic X-ray radiation and allows determination of energies of electronic levels based on the measured kinetic energies of the photoelectrons [22]. Phase composition was investigated using a Shimadzu XRD-7000S X-ray diffractometer with a K_αCu source with wavelength 1.54 Å. The degree of crystallinity was calculated as the ratio I_c/I_t, where I_c is the integrated diffraction intensity in the crystalline region and I_t is the total integrated intensity. The value of I_c was determined from the difference between I_t and I_a, where I_a is the integral intensity of the amorphous halo.

Water, ethylene glycol, and glycerol contact angles were measured by a sessile drop technique using a Kruss Easy Drop instrument. Contact angles were measured according to the Young-Dupree equation:

$$\sigma_{SG} = \sigma_{SL} + \sigma_{LG} cos\theta \quad (1)$$

where θ is the contact angle, and σ_{SG}, σ_{SL}, σ_{LG} are the surface tension coefficients at the solid-gas, solid-liquid, liquid-gas interfaces, respectively. Surface energy calculation was done using the Owens-Wendt equation [23]:

Table 1
The position and form of C1s and O1s lines in the PLA.

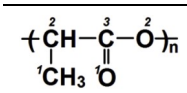	C1s			O1s	
	1	2	3	1	2
Binding energy, eV	285.00	286.98	289.06	532.25	533.66

$$\frac{\sigma_L \cdot (cos\theta + 1)}{2\sqrt{\sigma_L^D}} = \frac{\sqrt{\sigma_S^P} \cdot \sqrt{\sigma_L^P}}{\sqrt{\sigma_L^D}} + \sqrt{\sigma_S^D}, \quad (2)$$

where σ_L^D ,σ_S^D,σ_L^P, σ_S^P are the dispersion and polar components for the liquid and the solid, and σ_L is the total surface energy for the test liquid. Structural analysis was carried out by scanning electron microscopy using a Quanta 200 3D scanning electron microscope (SEM) and focused ion beam (FIB) instrument. Magnifications from 1000 to 15,000 were used at accelerating voltage of 20 kV, with spot size 2–3 nm. Before the SEM study, the samples were coated with a conducting gold film of 2–5 nm thickness by magnetron sputtering to alleviate charge build-up on the surface.

Microhardness of PLA, HA, PLA/HA 80/20 samples were measured with a Nanotest 600 hardness testing instrument using Berkovich tip at a load of 0.5 mN. Surface electrical resistivity (also called sheet resistance) was measured using an E6-13A teraohmmeter and calculated from the equation

$$\rho = Rb/l, \quad (3)$$

where R is the measured resistance, Ohm, $b = 3$ mm is the distance between the contacts, and $l = 10$ mm is the electrode length. Graflex plates pressed tightly to a polymer sample were used as the contacts (electrodes).

Analysis of macrophage survivability in culture was performed for evaluation of cytotoxicity of the investigated materials. The monocytes from the blood of three individual donors were isolated [24] using $CD14^+$ magnetic separation. Then monocytes were cultured in X–VIVO medium supplemented with cytokines and in the presence of the samples for 6 days at 37 °C at the atmosphere of 7.5% CO_2. Monocytes cultured without samples were used for control. On the sixth day of macrophage differentiation, the Alamar Blue indicator was added and the samples were incubated for another 3 h. Then, fluorescence response was measured [25]. As a negative control (no living cells), a X–VIVO serum-free medium with the addition of Alamar Blue (Alamar

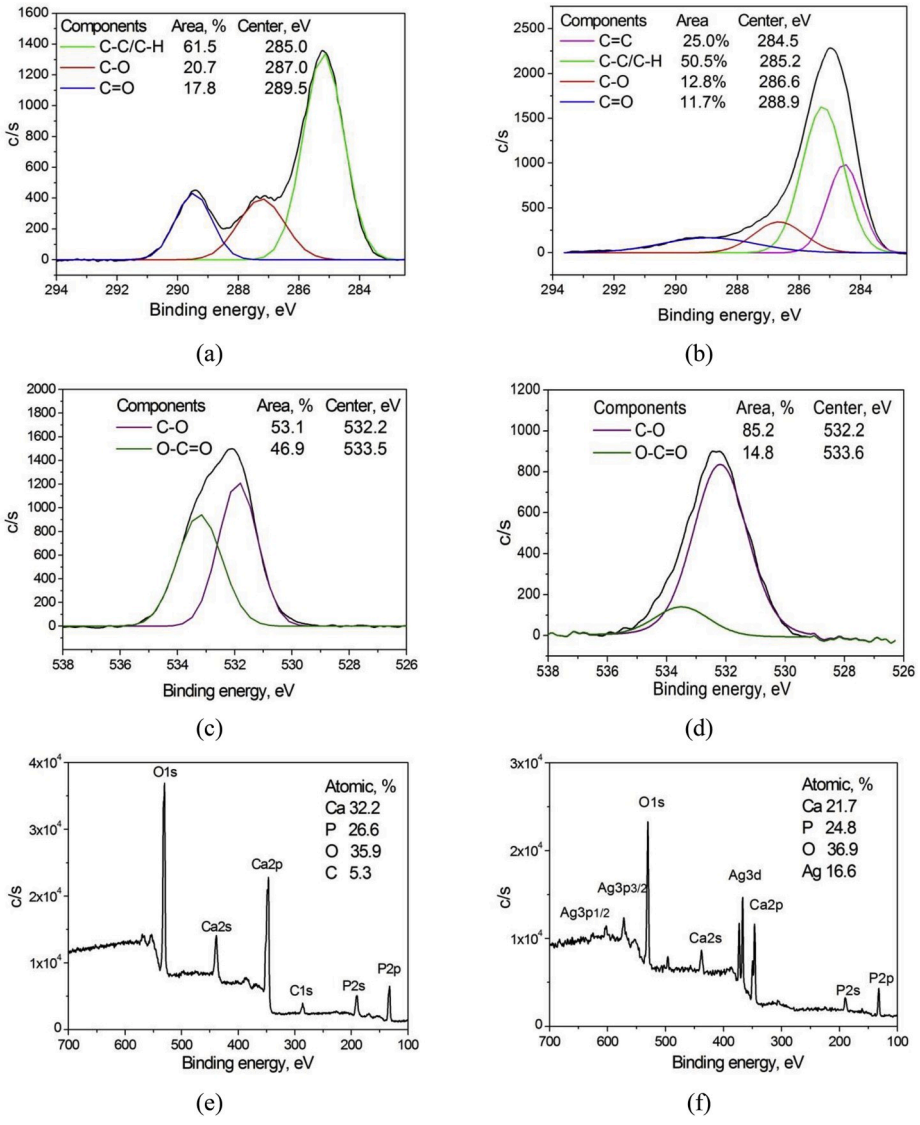

Fig. 2. XPS data of PLA and HA: a) C1s of the initial PLA, b) C1s of the PLA + Ag 1×10^{16} ion/cm^2, c) O1s of the initial PLA, d) O1s of the PLA + Ag 1×10^{16} ion/cm^2, e) survey spectrum of the initial HA, f) survey spectrum of the HA + Ag 1×10^{16} ion/cm^2.

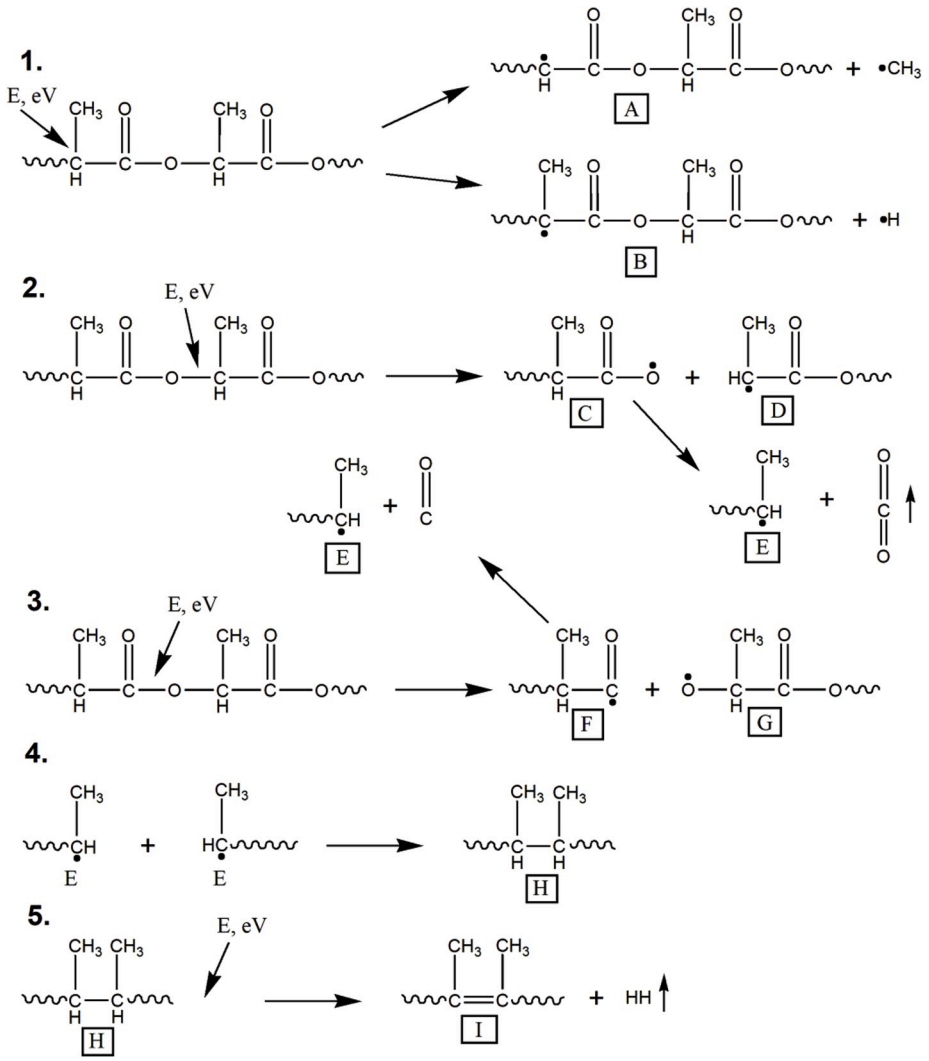

Fig. 3. Schemes of the chemical processes developing into the subsurface layer of PLA during Ag ion implantation.

Blue/medium ratio is 1/10) was used to measure the fluorescence signal, which was incubated for 3 h at 37 °C.

3. Results and discussion

3.1. Chemical and phase composition of PLA, HA and composite PLA/HA 80/20

Surface elemental composition of PLA, HA, composites of PLA/HA samples in the initial state and after silver ion implantation was investigated by X-ray photoelectron spectroscopy. Components detected in the C1s and O1s spectra are related to the chemical bonds in Table 1. In the initial PLA sample, the position and the shape of C1s and O1s lines correspond to the reference data on the binding energies in the PLA macromolecule (Fig. 2a and b, c, d). Table 1 represents the C1s and O1s spectra of the initial and implanted PLA surface.

Processes taking place in the surface layer of the polymer during ion implantation can be analyzed by comparison of C1s and O1s spectra of the initial and modified PLA. Surface carbonization is found to occur after Ag ion irradiation, the content of carboxyl group is decreased; the ratio of atomic concentration C/O is increased (C/O = 2.23 before the treatment; C/O = 5.18 after ion-beam modification) in the surface layer of PLA. A new line with the binding energy of 284.5, corresponding to sp^2 hybridization of carbon (-C═C-) appears in the C1s spectrum of Ag-implanted PLA. The π-bonds formation can be associated with destruction processes in the PLA macromolecules during accelerated ion interaction with the polymer chains. According to the XPS data, the following chemical reaction taking place during ion-beam treatment can be proposed (Fig. 3).

Firstly, free radicals (*A, B, C, D, F, G*) can be formed at the interaction of accelerated ions with the polymer surface in consequence of the polymer chain scission (Fig. 3, reactions **1**–**3**). Release of volatile monoxide and carbon dioxide is proposed to take place due to electron density shifts in radicals *C, F*. The free radicals *C, D, E, F, G* can recombine and form cross linking (*H*) as shown in Fig. 2, reaction **4**. During the action of incident ions with high energy, the formation of a π-bond (*I*) and the formation of a volatile hydrogen gas can be assumed as shown in Fig. 2, reaction **5**.

According to the XPS data for HA samples (Fig. 2e and f), it was found that silver ion irradiation results in the decrease of the atomic concentration of Ca and P, the ratio of Ca/P for the initial HA is 1.21, and after ion treatment – 0.87.

Fig. 4 shows XPS data for C1s, O1s, and survey spectra of the initial and 1×10^{16} ion/cm^2 Ag implanted PLA/HA 80/20 samples. The C1s spectra of the initial and modified ions surfaces of PLA/HA 80/20 samples contain carbon lines in three coordination states corresponding to the PLA (Table 1). In the surface layer of PLA/HA 80/20 after silver ion implantation the decrease of the content of –C═O bonds up to 2.7 times into the C1s spectrum and up to 1.8 times into the O1s spectrum is observed, which may be associated with parallel processes of

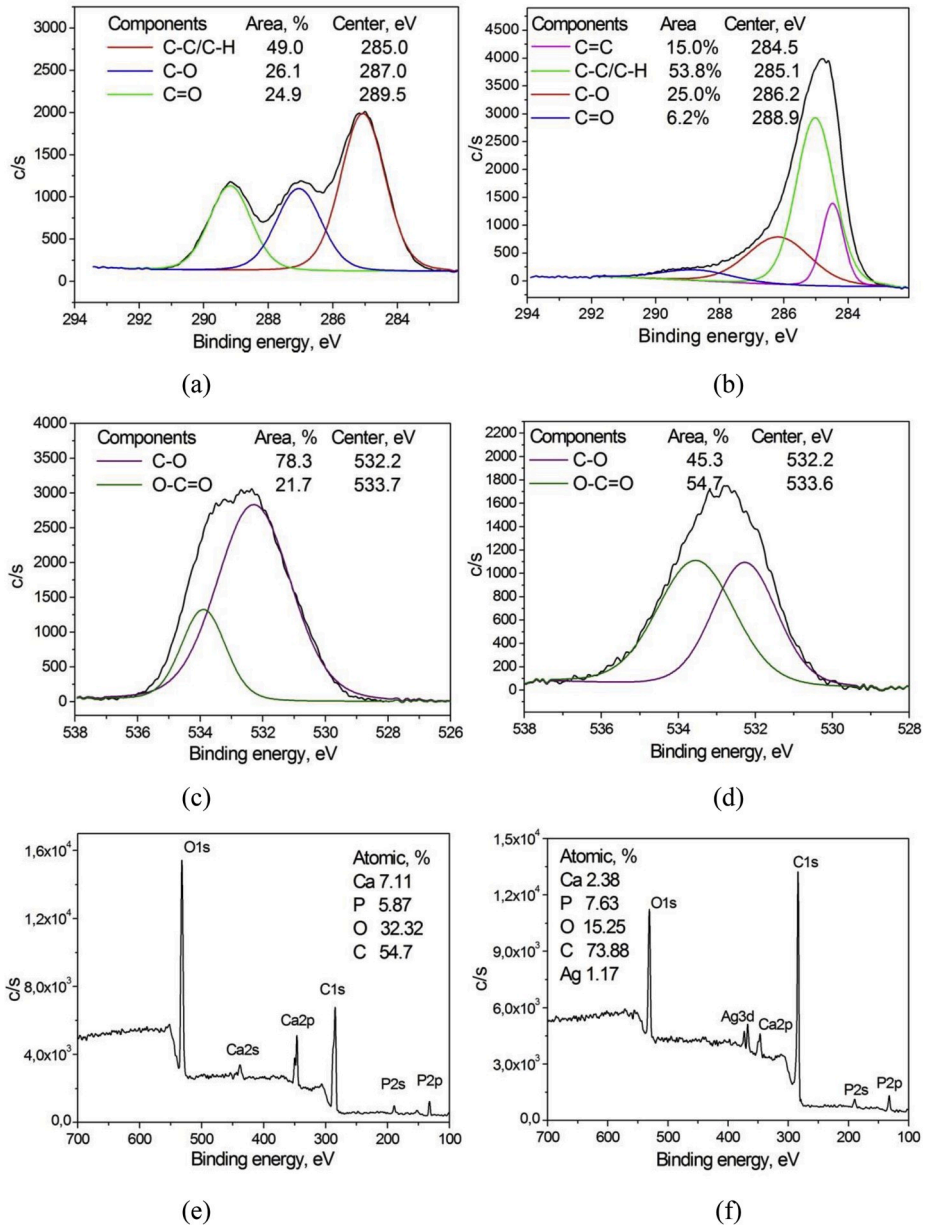

Fig. 4. XPS data of PLA/HA 80/20: a) C1s of the initial PLA/HA 80/20, b) C1s of the PLA/HA 80/20 + Ag 1 × 10^{16} ion/cm^2, c) O1s of the initial PLA/HA 80/20, d) O1s of the PLA/HA 80/20 + Ag 1 × 10^{16} ion/cm^2, e) survey spectrum of the initial PLA/HA 80/20, f) survey spectrum of the PLA/HA 80/20 + Ag 1 × 10^{16} ion/cm^2.

Table 2
Atomic concentration in the PLA, HA, PLA/HA samples according XPS data.

Sample	Atomic concentration of elements, at.%					
	C	O	Ca	P	Ag	Ca/P
PLA initial	68.03	31.97	–	–	–	–
PLA + Ag 1 × 10^{16} ion/cm^2	84.4	15.1	–	–	0.5	–
HA initial	–	39.24	34.5	26.26	–	1.31
HA + Ag 1 × 10^{16} ion/cm^2	–	35.74	24.87	27.46	11.93	0.91
PLA/HA initial	54.7	32.32	7.11	5.87	–	1.18
PLA/HA + Ag 1 × 10^{16} ion/cm^2	73.88	15.88	2.38	7.63	1.17	0.31

destruction and cross-linking during ion implantation. It should be noted that ion beam treatment leads to the calcium content decrease in the surface layer, which may be due to the effects of sputtering and knocking out of calcium ions from the surface layer (Fig. 4e and f, Table 2).

The XPS results indicate an increase in the atomic concentration of carbon on the surface of polylactic acid and composite PLA/HA (Table 2), which is due to the breaking of the polymer chains and, probably, the formation of carbon (graphite) clusters. In addition, the stoichiometry of hydroxyapatite was found to be changed after implantation with silver ions. The calculated atomic concentration ratio of Ca/P (Table 2) indicates that the experimental hydroxyapatite refers to octocalcium phosphate [26–28].

XPS data show that surface layers of the investigated materials contain silver atoms after Ag ion implantation (Table 2); herewith the maximum atomic concentration of silver is registered for hydroxyapatite since this material contains pores. Silver after ion implantation was established to be in the metallic state, without forming chemical bonds with other atoms of the polymer and non-organic matrixes (Fig. 5). The binding energy (E_b ($Ag3d_{5/2}$) = 368.0 eV, E_b ($Ag3d_{3/2}$) = 374.1 eV) of silver atoms corresponds to the electrons at the 3d level of silver in zero oxidation state (metallic state of silver). The difference in peak areas in the XPS results for PLA, HA and PLA/HA samples is explained by

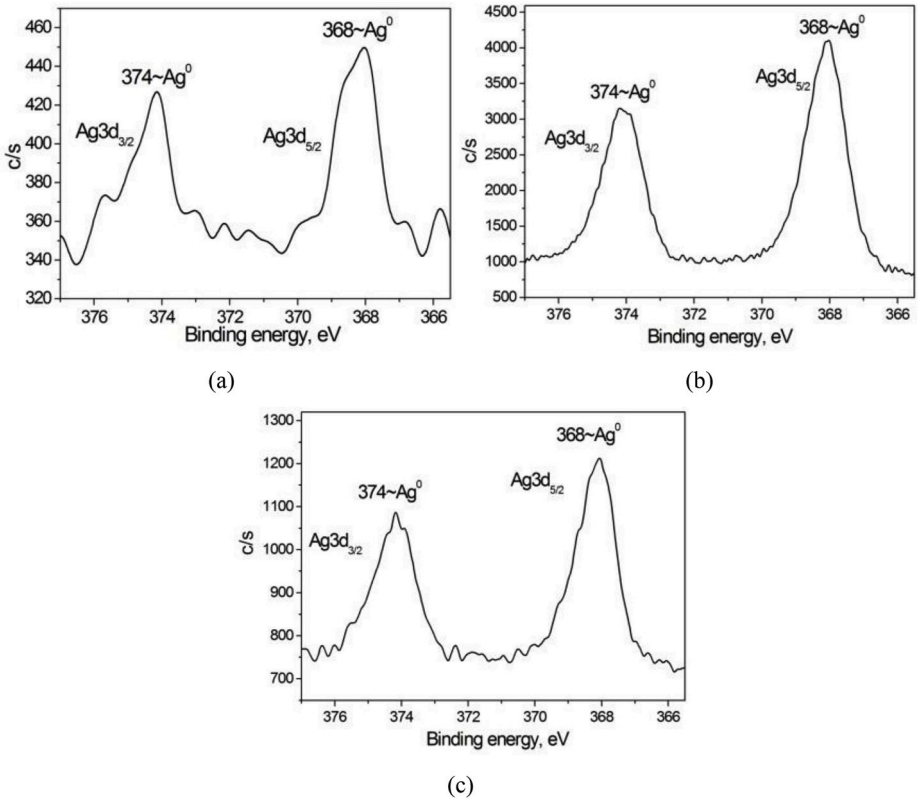

Fig. 5. Ag3d spectra of a) polylactic acid, b) hydroxyapatite, c) composite PLA/HA 80/20.

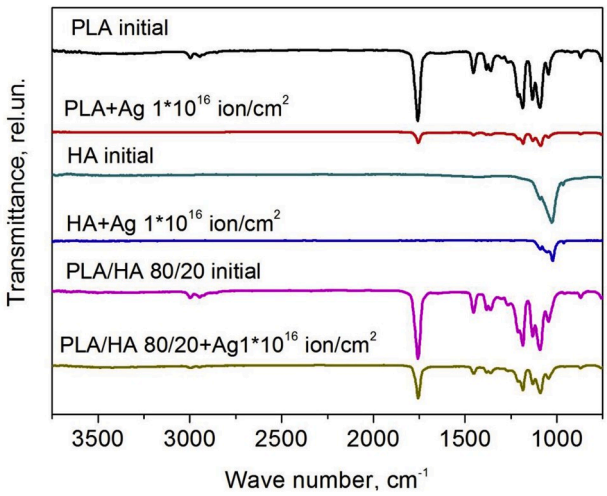

Fig. 6. IR-spectra of the initial and 1 × 10^{16} ion/cm^2 Ag-implanted PLA, HA, PLA/HA samples.

different densities of the materials.

The chemical composition of polylactic acid, hydroxyapatite, and composite PLA/HA before and after silver ion-beam treatment was studied using infrared spectroscopy. In the IR-spectrum of PLA (Fig. 6), the functional groups of -CH_3, -CH are corresponded by the stretching vibrations with wave numbers of 2944 cM-^{1} (symmetrical vibrations) and 2996 cM^{-1} (asymmetrical vibrations). In addition IR-spectrum of PLA contains stretching vibrations of the carbonyl group (–C═O) with the corresponding wave number of 1759 cM^{-1}. There are stretching vibrations of (–C(=O)–O) group with wave numbers of 1456, 1186, 1093, 1045 cM^{-1}. Deformation vibrations of a functional group (–C–O–C–) with a wave number 872 cM^{-1} are present as well.

Table 3
Characteristic vibration absorption bands in the IR-spectra of PLA, HA, and composite PLA/HA 80/20.

Group name	Wave number, cm^{-1}
ν (–C = O)	1760–1750
ν (–CH_3, –CH)	2995-2945, 2885-2980
δ (–CH_3)	1380–1360
ν (–O–H)	3500–2500
ν (PO_4^{3-}))	1030-1080, 960
δ (PO_4^{3-})	630, 600, 570
ν (–C–O–C–)	1150-1060, 1075–1020, 920-800

Displacement or the presence of new bands in the IR spectra of PLA was not detected. According to the IR spectroscopy results, the spectra of Ag-implanted PLA samples was found to be identical to the initial one (Fig. 6), they contain absorption bands corresponding to the PLA functional group vibrations.

Fig. 6 shows that in the IR-spectra of hydroxyapatite, both in the initial state and after ion implantation, four absorption bands in the region of 965, 1025, 1055 and 1087 cm^{-1}, corresponding to the stretching vibrations of the orthophosphoric groups PO_4^{3-} were observed. A decrease in the PO_4^{3-} line intensity after silver ion implantation was detected. According to the IR-spectroscopy data analysis, the spectra of the initial and Ag-implanted PLA/HA 80/20 samples contain bands characteristic for both PLA and HA (Fig. 6, Table 3). Moreover, a decrease in the intensity of characteristic lines of all materials is observed after ion-beam treatment, which is probably due to the formation of silver particles in the pores of the samples, since the oscillation of the pure metal is inactive in the IR-region.

The phase composition of the initial and Ag-implanted polylactic acid, hydroxyapatite, and composite PLA/HA was studied by X-ray phase analysis. Diffraction patterns of the initial and Ag-implanted PLA samples, which are shown in Fig. 7, contain two main peaks corresponding to angles 2Θ ≈ 19.1° and 16.9° and crystallographic planes

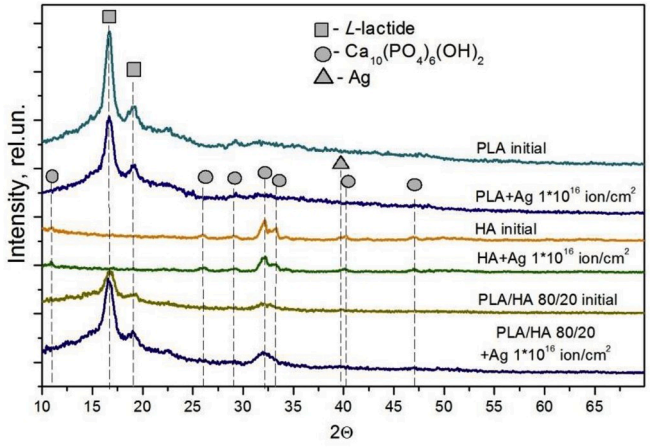

Fig. 7. Diffraction patterns of the initial and 1×10^{16} ion/cm^2 Ag-implanted.

Table 4
XRD data for the initial and Ag-implanted PLA, HA, PLA/HA samples.

Sample	XRD-analysis		
	Coherent scattering region	Degree of crystallinity	
		PLA	HA
PLA initial	13	63	–
PLA + Ag 1×10^{15} ion/cm^2	17	70	–
PLA + Ag 1×10^{16} ion/cm^2	19	74	–
HA initial	20	–	95
HA + Ag 1×10^{15} ion/cm^2	19	–	96
HA + Ag 1×10^{16} ion/cm^2	12	–	100
PL/HA initial	13	63	81
PLA/HA + Ag 1×10^{15} ion/cm^2	9	75	76
PLA/HA + Ag 1×10^{16} ion/cm^2	24	68	70

with indices (2 0 1), (1 1 0), characteristic for the structure of the L-isomer of polylactic acid. A change of the crystallographic parameters of the PLA after implantation is observed. The degree of crystallinity of polylactic acid after silver ion implantation increases from 68% to 74%, at the same time, the sizes of crystallites (areas of coherent scattering) change from 13 nm to 19 nm with the fluence increasing from 1×10^{15} to 1×10^{16} ion/cm^2. The degree of crystallinity is one of the main factors affecting the biodegradability of polymers, since complex protein molecules and various complexes that accelerate chemical reactions in a living organism mainly break down the amorphous regions of the material. Polymer molecules in the amorphous regions are less densely packed, so the material is more susceptible to decomposition. It is known that the rate of biodegradation with increasing degree of crystallinity of the polymer decreases [29].

Diffraction patterns of the initial and Ag-implanted hydroxyapatite samples (Fig. 7) contain the peaks corresponding to the monoclinic syngony of the composition $Ca_{10}(PO_4)_6(OH)_2$ with the following angles 2Θ and crystallographic planes: 10.8° → (1 0 0), 25.8°→(0 0 2), 28.9°→(2 1 0), 31.7°→(1 1 2), 32.9°→(3 0 0), 39.8°→ (1 3 0), 40.4°→(2 2 1), 46.7°→(2 2 2). Ion implantation has no influence on the positions and shapes of the diffraction maxima in HA.

According to the X-ray phase analysis, the diffraction patterns of composite PLA/HA 80/20 before and after ion implantation contain reflexes typical of both polylactic acid and hydroxyapatite. Two diffraction lines are typical for PLA: 2Θ = 16.6°; 19.1 °. Hydroxyapatite is characterized by the following set of diffraction lines: 2Θ = 25.8°, 31.7°; 32.9°. The crystallographic parameters correspond to the hydroxyapatite of the composition $Ca_{10}(PO_4)_6(OH)_2$. It was found that, there are no new reflections and shifts of diffraction lines after ion implantation, which indicates the preservation of the phase composition

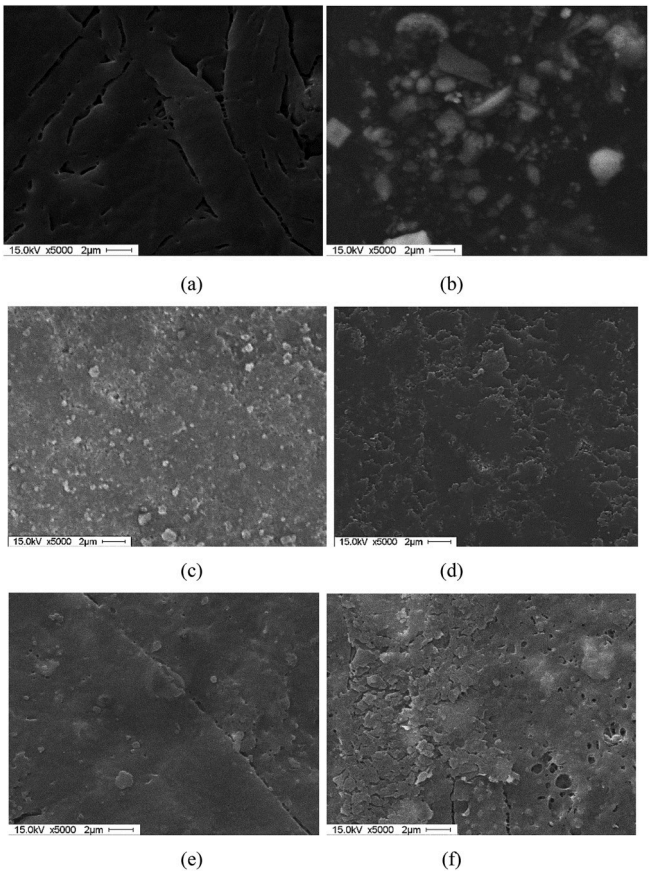

Fig. 8. SEM-images of the initial and Ag-implanted PLA, HA, PLA/HA samples: a) initial PLA, b) PLA + Ag 1×10^{16} ion/cm^2, c) initial HA, d) HA + Ag 1×10^{16} ion/cm^2, e) initial PLA/HA 80/20, f) PLA/HA 80/20 + Ag 1×10^{16} ion/cm^2.

and crystallographic identity of the original components. The degree of crystallinity of composite PLA/HA increases from 63% to 68% after Ag ion implantation (Table 4). It has been shown that in semi-crystalline polymers irradiated with high-energy ions, a decrease in the degree of amorphization is observed [30]. This phenomenon is due to several factors. For example, radiation causes compression of polymer chains during propagation of ions through the polymer, thereby reducing the volume of pores inside it. In this work, after irradiation of the surface of the composites with silver ions, an increase in the porosity of the surface layers of the polymer is observed (Fig. 8, e). In addition, irradiation leads to increase of crystallite size due to radiation heating [31]. Another factor could be the rearrangement of macromolecules dangling during irradiation at the interface between the amorphous and crystalline phases [32].

3.2. Morphology and wettability

Fig. 8 shows micrographs of the surface of the PLA obtained by scanning electron microscopy. The result of ion implantation is a change in the morphology and surface topography of polylactic acid. In the 1×10^{16} ion/cm^2 Ag-implanted PLA subsurface layer (Fig. 8, b), metallic silver particles were detected. According to the TEM results, it was found that when irradiated with silver ions, metallic nanoparticles with an average size of 2–3 nm are formed in the surface layer of the PLA [14]. According to the SEM data, pores are formed on the surface of PLA/HA 80/20 composites after implantation with silver ions.

It is known that wettability plays an important role in biochemical processes occurring on the "bond tissue-liquid" interface. Measurements of PLA surface contact angle were carried out by the sessile drop methods at the contact with three liquids: water, glycerol, and ethylene

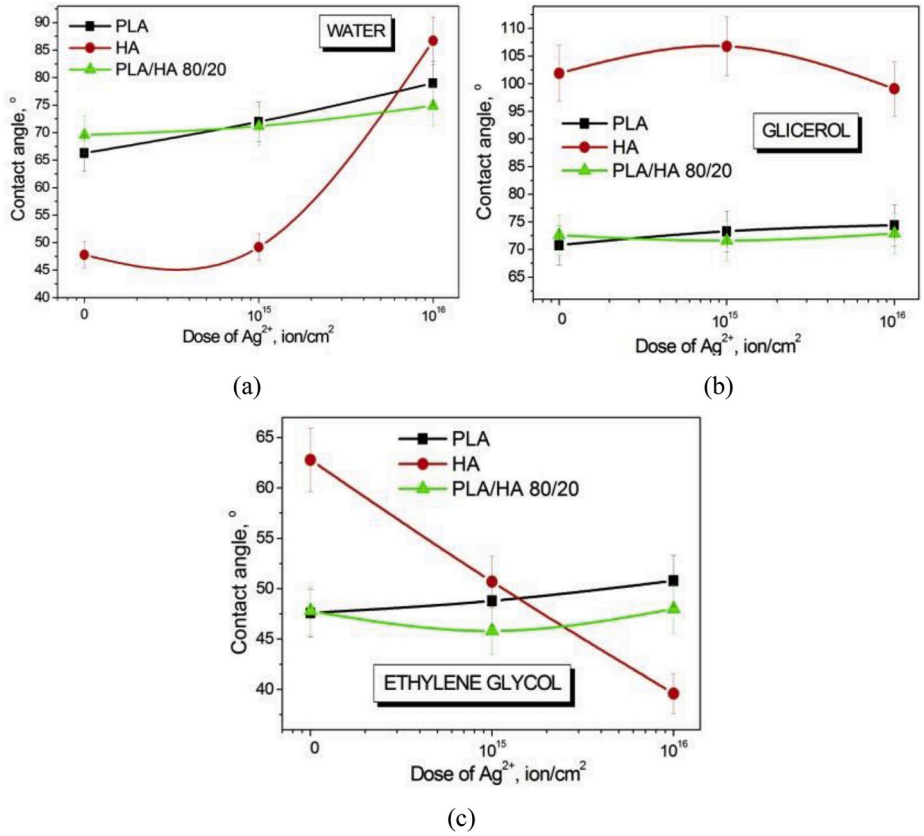

Fig. 9. Contact angles of PLA, HA, and composite PLA/HA 80/20 at the contact with a) water, b) glycerol, c) ethylene glycol.

Table 5
Surface energy and its components for PLA, HA, PLA/HA 80/20.

Sample	Surface energy, mN/m		
	Polar	Dispersion	Total
PLA initial	31.16 ± 1.07	5.15 ± 0.38	36.30 ± 1.45
PLA + Ag 1 × 10^{15} ion/cm^2	21.46 ± 0.93	9.45 ± 0.62	30.91 ± 1.55
PLA + Ag 1 × 10^{16} ion/cm^2	12.95 ± 0.68	13.95 ± 0.69	26.90 ± 1.37
HA initial	79.4 ± 3.99	1.01 ± 0.15	80.96 ± 4.04
HA + Ag 1 × 10^{15} ion/cm^2	60.79 ± 3.03	0.75 ± 0.11	61.53 ± 3.07
HA + Ag 1 × 10^{16} ion/cm^2	6.89 ± 0.34	15.7 ± 2.35	22.59 ± 1.12
PL/HA initial	19.88 ± 1.07	12.85 ± 0.79	32.73 ± 1.86
PLA/HA + Ag 1 × 10^{15} ion/cm^2	12.86 ± 0.80	23.54 ± 1.10	36.40 ± 1.89
PLA/HA + Ag 1 × 10^{16} ion/cm^2	13.91 ± 0.74	16.71 ± 0.84	30.62 ± 1.58

glycol. For the ion implanted PLA samples, a linear tendency to the contact angle increase with the fluence was observed in the case of contact with water and ethylene glycol (Fig. 9a and b). In total, the material became more hydrophobic after ion implantation.

Table 6
Functional characteristics of polylactic acid, hydroxyapatite, and composite PLA/HA 80/20 samples before and after silver ion implantation.

Sample	Functional properties	
	Microhardness, MPa	Surface resistivity, Ohm
PLA initial	510	1.3 × 10^{13}
PLA + Ag 1 × 10^{15} ion/cm^2	340	6.3 × 10^{11}
PLA + Ag 1 × 10^{16} ion/cm^2	310	5.4 × 10^{7}
HA initial	340	5.4 × 10^{7}
HA + Ag 1 × 10^{15} ion/cm^2	270	4.5 × 10^{7}
HA + Ag 1 × 10^{16} ion/cm^2	228	1.2 × 10^{8}
PLA/HA initial	320	7.2 × 10^{12}
PLA/HA + Ag 1 × 10^{15} ion/cm^2	330	6.7 × 10^{9}
PLA/HA + Ag 1 × 10^{16} ion/cm^2	430	2.2 × 10^{7}

Hydroxyapatite is a moisture-absorbing material; therefore, several contact angle measurements on its surface were carried out for 3 s after drop application, average volumes were taken. A strong tendency to water angle enhancement from 47° to 86° (Fig. 9, a) with increase of the ion fluence was observed for silver implanted hydroxyapatite. In the initial state, hydroxyapatite is oleophobic material, the contact angle with glycerol is 102° (Fig. 9, b). The values of glycerol contact angle for ion implanted hydroxyapatite are slightly different from the initial one. When HA samples are wetted with ethylene glycol, a linear tendency to contact angle decrease from 63° to 40° is observed, hence the material becomes more hydrophilic (Fig. 9, c). The values of contact angles for composite material PLA/HA 80/20 are similar to pure PLA ones, the same tendencies occur: the contact angles of ion implanted PLA/HA 80/20 samples slightly enhance when wetted with all the liquids (water, glycerol, ethylene glycol) (Fig. 9a and b, c).

Surface energy contains two components: dispersion (van der Waals forces and other non-specific interactions) and polar (strong interactions between surface atoms and adsorbed liquid molecules and hydrogen forces). It was established that silver ion implantation of PLA samples leads to a decrease in the polar part and an increase in the dispersion component, while the total surface energy of the PLA decreases from 36.3 mN/m to 26.9 mN/m with increase of the fluence (Table 5).

It should be noted that the total surface energy of hydroxyapatite is decreased from 80.96 mN/m to 22.59 mN/m with the silver ion fluence increasing to 1 × 10^{16} ion/cm^2. This is accompanied by an increase in the dispersion component and decrease in the polar component (Table 5). It was established that the polar component of the surface energy of the silver ion implanted PLA/HA 80/20 decreases and the dispersion component increases (Table 5), while the total surface energy does not undergo significant changes.

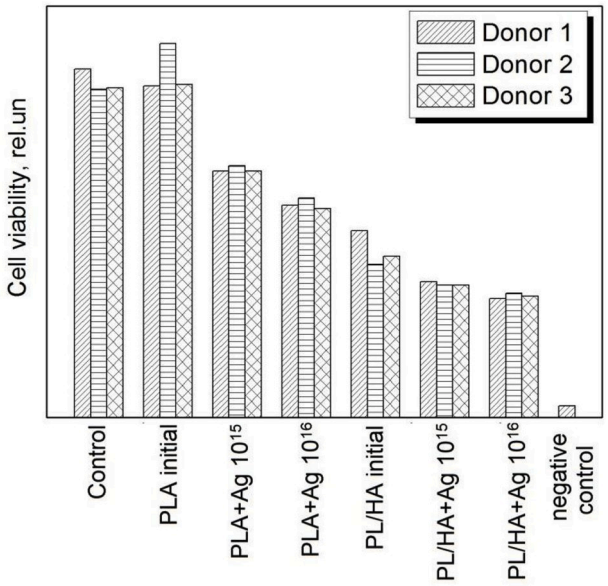

Fig. 10. Evaluation of primary monocytic macrophages viability in the presence of the PLA, HA, PLA/HA 80/20 initial and 1×10^{15}, 1×10^{16} ion/cm^2 silver ion implanted samples.

3.3. Functional properties

Physical-mechanical properties such as microhardness and surface resistivity are significant for the quality evaluation of materials for biomedical applications. Microhardness values of the initial and ion implanted PLA, HA, PLA/HA 80/20 samples at the load of 0.5 mN are presented in Table 6. The microhardness of PLA after ion implantation is established to be decreased by the factor of 1.5 in comparison with the initial state. The decrease in microhardness can be associated with an increase in the amorphous regions, as well as with processes of macromolecule destruction. Under the influence of ion irradiation on polymers an intensive thermal action takes place, which leads to the restructuring of the material and the degree of crystallinity decreasing. Silver ion bombardment is shown to be resulted in HA microhardness decrease from 340 MPa to 228 MPa while fluence increasing. The initial value of microhardness for PLA/HA 80/20 composite material is approximately congruent to the initial PLA one due to small content of calcium phosphate component. When silver ion treatment of the composite, the enhancement of microhardness from 320 MPa to 430 MPa at the fluence of 1×10^{16} ion/cm^2 is observed.

Surface resistivity of the initial PLA is 1.3×10^{13} Ohm. Silver ion implantation leads to the PLA surface resistivity decrease by the factor of 5 ($\rho = 5.4 \times 10^7$ Ohm). Surface resistivity of polylactic acid-hydroxyapatite-based composite undergoes similar changes as pure polylactic acid one. The conductivity of PLA/HA 80/20 composites increases by orders of magnitude with the fluence increase. It should be noted that surface resistivity of the initial HA is minimal for the investigated materials ($\rho = 5.4 \times 10^7$ Ohm). It was found that silver ion implantation does not influence significantly the HA surface resistivity, it changes within the same order. Table 6 reveals the tendency to the surface resistivity decrease with the non-organic component enhancement in the composite content. The implanted silver ions form the metallic particles which promote the electrical conductivity enhancement. On the other hand, ion implantation contributes to the increase in the content of carbon atoms in polylactic acid (Table 2). Hence, the two factors contribute to the increase in electrical conductivity: the formation of metal clusters and the increase in atomic concentration of carbon, which is an electrically conductive.

Cytotoxicity analysis *in vitro* of macrophages after adding of the test samples (Fig. 10) reveals that cell viability in the presence of the initial PLA is comparable to the control sample (silicon glass). Negative effect of hydroxyapatite in the PLA/HA composite on the viability of macrophages is observed. With the ion fluence increase, the viability of macrophages decreases in presence of all the samples (PLA, PLA/HA), but it still remains significantly higher than the negative control, most of the cells retain viability.

4. Conclusion

The effect of silver ion implantation at the fluence of 1×10^{15} and 1×10^{16} ion/cm^2 on the physicochemical and mechanical properties of polylactic acid, hydroxyapatite, and composite material of PLA/HA 80/20 has been investigated by several methods. It is shown that surface treatment with silver ions affects the energy state of the surface of the materials.

According to the XPS data, implanted silver forms metal nanoparticles in the subsurface layers of the polymer or hydroxyapatite matrixes. The bond ratios in the C1s spectra are changed due to polymer chain scission, cross-linking and oxidation processes during ion implantation. According to the IR-spectroscopy, the intensities of characteristic lines for all the investigated materials are decreased, which is probably due to the formation of silver particles in the pores of the samples. The degrees of crystallinity of polylactic acid, hydroxyapatite and composite PLA/HA 80/20 are increased after silver ion implantation.

Ion beam treatment contributes to a change in the surface wettability of polymer and composite materials at the contact with polar (water, ethylene glycol) and non-polar (glycerin) liquids. A linear tendency to the contact angle increase with the fluence increase is observed; therefore, the materials after ion implantation acquire hydrophobic properties. Moreover, the total surface energy of Ag-implanted materials is also decreased due to a change in the ratio of its components: the polar component of the surface energy decreases while the dispersion component becomes dominant. The microhardness values of PLA, HA and PLA/HA 80/20 were established to be decreased after the silver ion implantation with the fluence increasing, which is associated with the processes of destruction due to the polymer chain scission. Intense local thermal effects under the influence of ion irradiation on polymers and composites may leads to the restructuring of the material and the decrease in the regions with ordered arrangement of macromolecules. The surface resistivity reduces after silver ion implantation of polylactic acid and PLA/HA 80/20 composite by the factor of 5, which may be due to the formation of conductive clusters of metal and carbon on their surface. Cell viability is observed to be stable in the presence of the initial PLA sample and decreased in the presence of hydroxyapatite (HA) in the PLA/HA composite and after ion implantation for all the samples. Thus, ion implantation negatively affects the viability of macrophages.

Acknowledgments

This work was supported by the Tomsk State University Competitiveness Improvement Program under Grant. Special thanks are extended to the Center for Collective Use at National Research Tomsk State University and the Laboratory of Plasma Sources of the Institute of High Current Electronics, and particularly to Dr. Sci., Prof. E.M. Oks.

References

[1] D.V. Sviridov, Ion implantation in polymers: chemical aspects, Chem. Probl. Dev. New Mater. Technol. 1 (2003) 88–106. http://elib.bsu.by/bitstream/123456789/20977/1/pages%20from%20Sbornik-END7.pdf.

[2] V.N. Popok, Ion implantation of polymers: formation of nanoparticulate materials, Rev. Adv. Mater. Sci. 30 (2012) 1–26. http://www.ipme.ru/e-journals/RAMS/no_13012/01_popok.pdf.

[3] E. Sokullu-Urkac, A. Oztarhan, F. Tihminlioglu, A. Nikolaev, I. Brown, Oxidation behavior of C- and Au-Ion-Implanted biodegradable polymers, IEEE Trans. Plasma Sci. 40 (2012) 863–869, https://doi.org/10.1109/TPS.2011.2179677.

[4] E. Sokullu Urkac, A. Oztarhan, F. Tihminlioglu, N. Kaya, D. Ila, C. Muntele, S. Budak, E. Oks, A. Nikolaev, A. Ezdesir, Z. Tek, Thermal characterization of Ag and Ag + N ion implanted ultra-high molecular weight polyethylene (UHMWPE), Nucl. Instrum. Methods Phys. Res. B 261 (2007) 699–703, https://doi.org/10.1016/j.nimb.2007.04.102.
[5] J. Fang, J. Zhao, Y. Sun, H. Ma, X. Yu, Y. Ma, Y. Ni, L. Zheng, Biocompatibility and antibacterial properties of zinc-ion implantation on titanium, J. Hard Tissue Biol. 23 (2014) 35–44, https://doi.org/10.2485/jhtb.23.35.
[6] N. Akamatsu, Artifacial bone and joints, Asian Med. J. 36 (1993) 621–627.
[7] L. Hench, Bioceramics, J. Am. Ceram. Soc. 81 (1998) 1705–1728, https://doi.org/10.1111/j.1151-2916.1998.tb02540.x.
[8] A. Toth, K. Kereszturi, M. Mohai, I. Bertoti, Plasma based ion implantation of engineering polymers, Surf. Coat. Technol. 204 (2010) 2898–2908, https://doi.org/10.1016/j.surfcoat.2009.12.004.
[9] T.L. Schiller, D. Sheeja, D.R. McKenzie, D.G. McCulloch, D.S.P. Lau, S. Burn, B. K. Tay, Surf. Coating. Technol. 483 (2004) 177–178, https://doi.org/10.1016/S0257-8972(03)00916-2.
[10] A.Y. Song, Y.A. Oh, S.H. Roh, J.H. Kim, S.C. Min, Cold oxygen plasma treatments for the improvement of the physicochemical and biodegradable properties of polylactic acid films for food packaging, Food Eng. Mater. Sci. 81 (2015) 86–96, https://doi.org/10.1111/1750-3841.13172.
[11] S.I. Tverdokhlebov, E.N. Bolbasov, E.V. Shesterikov, L.V. Antonov, A.S. Golovkin, V.G. Matveev, D.G. Petlin, Y.G. Anissimov, Modification of polylactic acid surface using RF plasma discharge with sputter deposition of a hydroxuapatite target for increased biocompatibility, Appl. Surf. Sci. 329 (2015) 32–39, https://doi.org/10.1016/j.apsusc.2014.12.127.
[12] D.J. Leonard, L.T. Pick, D.F. Farrar, G.R. Dickson, J.F. Orr, F.J. Buchanan, The modification of PLA and PLGA using Electron-beam radiation, J. Biomed. Mater. Res. 89A (2008) 567–574, https://doi.org/10.1002/jbm.a.31998.
[13] J.S.C. Loo, C.P. Ooi, F.Y.C. Boey, Degradation of poly (lactide-coglycolide) (PLGA) and poly(-lactide) (PLA) by electron beam radiation, Biomaterials 26 (2005) 1359–1367, https://doi.org/10.1016/j.biomaterials.2004.05.001.
[14] I.V. Pukhova, K.P. Savkin, O.A. Laput, D.N. Lytkina, V.V. Botvin, A.V. Medovnik, I. A. Kurzina, Effects of ion- and electron-beam treatment on surface physicochemical properties of polylactic acid, Appl. Surf. Sci. 422 (2017) 856–862, https://doi.org/10.1016/j.apsusc.2017.06.112.
[15] YeG. Shapovalova, D.N. Lytkina, I.A. Kurzina, Y.G. Kzhyshkovska, Preparation of biocompatible composites based on poly-L-lactide/hydroxuapatite and investigation of their anti-inflammatory activity, Key Eng. Mater. 683 (2016) 475–480. https://doi.org/10.4028/www.scientific.net/KEM.683.475.
[16] D.N. Lytkina, A.A. Berezovskaya, N.M. Korotchenko, I.A. Kurzina, V.V. Kozik, Preparation of composite materials based on hydroxyapatite and lactide and glycolide copolymer, AIP Conf. Proc. 1899 (2017), https://doi.org/10.1063/1.5009840, 020015-1–020015-6.
[17] N.M. Korotchenko, L.A. Rasskazova, The Method of Obtaining Silicon-Modified Hydroxuapatite Using Microwave Radiation (NR TSU) Ru, 2014, p. 2507151 (in Russian).
[18] V.A. Syusyukina, Y.G. Shapovalova, N.M. Korotchenko, I.A. Kurzina, Structural-phase state and surface properties of composite materials based on polylactide and hydroxyapatite, Russ. J. Appl. Chem. 90 (2017) 106–112, https://doi.org/10.1134/S1070427217010165.
[19] I.G. Brown, The metal vapor vacuum arc (MEVVA) high current ion source, IEEE Trans. Nucl. Sci. 32 (1985) 1723–1727, https://doi.org/10.1109/TNS.1985.4333703.
[20] K.P. Savkin, E.M. Oks, V.I. Gushenets, V.P. Frolova, A.G. Nikolaev, G.Yu Yushkov, Vacuum arc ion source with compound cathode and beam separation by bending magnet, in: 27th International Symposium on Discharges and Electrical Insulation in Vacuum (ISDEIV), 2016. https://ieeexplore.ieee.org/document/7764029.
[21] V.I. Gushenets, A.G. Nikolaev, E.M. Oks, L.G. Vintizenko, G.Yu Yushkov, Simple and inexpensive time-of-flight charge-to-mass analyzer for ion beam source characterization, Rev. Sci. Instrum. 77 (2006), https://doi.org/10.1063/1.2206778, 063301-1-063301-3.
[22] M. Inagaki, F. Kang, Materials Science and Engineering of Carbon: Characterization, Elsevier Inc., 2016, pp. 153–171.
[23] J. Bico, U. Thiele, D. Quere, Wetting of textured surfaces, Colloid. Surface. Physicochem. Eng. Aspect. 206 (2002) 41–46, https://doi.org/10.1016/S0927-7757(02)00061-4.
[24] A. Gratchev, M1 and M2 can be re-polarized by Th2 or Th1 cytokines respectively, and respond to exogenous danger signals, Immunobiology 211 (2006) 473–486, https://doi.org/10.1016/j.imbio.2006.05.017.
[25] S. Al-Nasiry, N. Geusens, M. Hanssens, C. Luyten, R. Pijnenborg, The use of Alamar Blue assay for quantitative analysis of viability, migration and invasion of choriocarcinoma cells, Hum. Reprod. 22 (5) (2007) 1304–1309, https://doi.org/10.1093/humrep/dem011.
[26] M. Bohner, Calcium orthophosphates in medicine: from ceramics to calcium phosphate cements, Injury 31 (2000) 37–47, https://doi.org/10.1016/S0020-1383(00)80022-4.
[27] P. Layrolle, Sol–gel synthesis of amorphous calcium phosphate and sintering into microporous hydroxyapatite bioceramics, J. Am. Ceram. Soc. 81 (1998) 1421–1428, https://doi.org/10.1111/j.1151-2916.1998.tb02499.x.
[28] R.Z. Legeros, S. Lin, R. Rohanizadeh, D. Mijares, J.P. Legeros, Biphasic calcium phosphate bioceramics: preparation, properties and applications, J. Mater. Sci. Mater. Med. 14 (2003) 201–209. https://doi.org/10.4028/www.scientific.net/kem.240-242.473.
[29] B.P. Calabia, Y. Tokiwa, C.U. Ugwu, S. Aiba, Biodegradation, Poly(Lactic Acid): Synthesis, Structures, Properties, Processing, and Applications, John Wiley & Sons Inc., Hoboken, 2010, pp. 423–430, https://doi.org/10.1002/9780470649848.ch25.
[30] B. Mallick, S. Panigrahi, Effect of amorphization cross-section of polymer due to MeV-proton irradiation, Appl. Phys. 1 (2012) 20–25. https://www.researchgate.net/publication/237098990.
[31] M. Olvera-Gracia, J.R. Aguilar-Hernandez, Conductivity and crystallinity of polyethylene oxide/polyaniline microfibers obtained by electrospinning, J. Appl. Res. Technol. 12 (2014) 598–601, https://doi.org/10.1016/S1665-6423(14)71638-4.
[32] S. Kim, Y.C. Nho, Effect of Radiation on Ultra High Molecular Weight Polyethylene (UHMWPE), Controlling of Degradation Effects in Radiation Processing of Polymers, IAEA, Vienna, 2009, pp. 85–95, in: https://www.iaea.org/publications/8063/controlling-of-degradation-effects-in-radiation-processing-of-polymers.